Laser melting of nano-crystalline uranium dioxide

F. Cappia [a,b], R. Jovani-Abril [a], J. Spino [a], L. Luzzi [b], A. Janßen [a], D. Manara [a,*]

[a] European Commission, Institute for Transuranium Elements, JRC-ITU, P.O. Box 2340, 76125 Karlsruhe, Germany
[b] Politecnico di Milano – Department of Energy CeSNEF (Enrico Fermi Center for Nuclear Studies), via Ponzio, 34/3, 20133 Milan, Italy

Article history:
Received 18 October 2013
Accepted 21 October 2013

1. Introduction

1.1. Particular properties of sub-micrometric-sized high-burn-up structure

Recent research has shown that the peripheral region of the fuel which has undergone re-crystallization (or "polygonization") in the nanometre-size range under high burn-up (also called "High Burn-up Structure" or HBS) (Rondinella and Wiss, 2010) presents increased fission gas retention and ameliorated mechanical properties without sensibly reducing the thermal conductivity (Rondinella and Wiss, 2010; Spino et al., 2012, 1996, 2003; Ronchi et al., 2004). All these advantages have suggested the possibility to use in the future nano-crystalline (nc) actinide oxides as advanced fuels (Spino et al., 2012). The best grain size for such potential application has been estimated to be between approximately 100 nm and 300 nm, emulating the HBS features (Spino et al., 2012). According to the exploratory research performed so far, this grain size range constitutes a good compromise between the aforementioned advantageous aspects deriving from the small structure and the possible deterioration of thermal properties due to grain boundary effects (Spino et al., 2012).

In this context, main goal of the present work is to explore the melting behaviour of nano-structured UO_2, already studied up to approximately 1500 K by X-ray diffraction and dilatometry (Jovani-Abril et al., 2011). Both thermal conductivity and melting temperature can be affected when the material's average grain size is at the nanometric scale ($\leq 10^{-7}$ m or 100 nm). The increased number of grain boundaries can be associated to increased effects of thermal boundary resistance, whereas melting point depression is a well-known phenomenon for free nanoparticles (Roduner, 2006; Mei and Lu, 2007; Hill, 2001; Guisbiers, 2012; Takagi, 1954; Buffat and Borel, 1976; Lai et al., 1996, 1998; Wronski, 1967; Coombes, 1972).

1.2. Melting of nano-structured materials

This latter effect can be explained with the help of classical thermodynamics. Because a nano-structured nuclear fuel element contains a macroscopic amount of nano-sized objects (nano-grains or particles), it can be seen as a large ensemble of nanoscopic systems (Roduner, 2006; Mei and Lu, 2007; Hill, 2001; Guisbiers, 2012) from a thermodynamic viewpoint. Thus, its behaviour can still be explained by the basic thermodynamic equations of macroscopic systems by adding some corrections which take into account the finite-size of the system. For example, the stable states of the system are no longer governed by the sole volumic Gibbs energy $G_V(T)$, but a generalised Gibbs energy $G^*(T)$ must be used to take into account contributions from both the particle volume and the free surfaces or interfaces:

$$G^*(T) = G_V(T) + G_{S/I}(T) \quad (1)$$

In Eq. (1), $G_{S/I}(T)$ is the surface energy (surface tension) of the particle or the interfacial energy between the particle and the substrate/host matrix (e.g.: a ligand).

Considering the solid-liquid transition, the melting temperature is defined as the temperature at which the Gibbs energy of the solid

* Corresponding author. Tel.: +49 7247 951 129.
E-mail addresses: fabiola.cappia@ec.europa.eu (F. Cappia), dario.MANARA@ec.europa.eu (D. Manara).

phase ($G_S(T)$) is equal to the Gibbs energy of the liquid phase ($G_L(T)$). In a micro- or macro-structured solid this condition is expressed by the identity $G_V(T) = G_L(T)$, because $G_S(T) = G_V(T)$ with very good approximation since $G_{S/l}(T) \approx 0$. When a nano-structured solid is considered instead, the total energy of the solid phase is expressed by Eq. (1), and the new equilibrium temperature is defined by $G^*(T) = G_L(T)$. According to the relative contribution of the second term in the right hand side of Eq. (1), either melting point depression or superheating (i.e., an increase in the melting temperature) can be observed. However, a depression of the fusion/solidification point is mostly observed in high-melting materials (such as the current oxides, but also many metals), due to the fact that they are generally free from any hosting matrix when heated to high temperatures. The thermodynamic theory of small particle melting has been developed in depth elsewhere (Roduner, 2006; Mei and Lu, 2007; Hill, 2001; Guisbiers, 2012).

All models used to predict the melting temperature variation establish a universal relation between melting temperature and grain size, which is a generalisation of the Gibbs-Thompson equation (Guisbiers, 2012):

$$\frac{T_m}{T_{m,\infty}} \propto 1 - \frac{\alpha}{D} \tag{2}$$

The symbols used in Eq. (2) are: $T_m/T_{m,\infty}$ the ratio of nanoparticles and bulk material melting temperatures, D the nanoparticle average diameter and α a constant representing the thermophysical properties of the material and depending on the model used.

Of course, a decrease in the melting temperature of a nuclear fuel would reduce its margin-to-melting safety parameter (Olander, 1976). The solid/liquid transition of the current nano-structured oxide constitutes therefore a paramount subject of study. It is essential for the definition of the safety and performance limits of the potential advanced fuel which might in the future be based on such material.

Although the melting behaviour of rather numerous nano-structured materials has already been investigated, the present study is the first, to the authors' knowledge, to explore the solid-liquid transition in high-melting, refractory materials. In particular, bulk UO_2 is known to melt at 3120 K ± 30 K (Manara et al., 2005), nearly two thousand K above the melting point of gold, the highest-melting material for which the solid-liquid transition has been studied both in nano- and micro- or macro-structured samples (Buffat and Borel, 1976). The present research deals with crystallites whose size is a few tens of nm. Crystallites in this size range have sometimes been observed in the high burn-up structure (Nogita and Une, 1994), although they are significantly smaller than the mean grain sizes proposed by Spino et al. for a potentially nano-structured nuclear fuel (Spino et al., 2012). The goal of this first investigation actually consists in checking the existence and the extent of any detectable size effects on a grain-size scale where such effects have been observed in other kind of materials (Takagi, 1954; Buffat and Borel, 1976; Lai et al., 1996), and giving conservative performance limits for a fuel displaying, partly or entirely, the features observed in the HBS.

The only experimental approach currently available to perform such an experimental investigation on nano-structured high-melting refractory oxide is laser heating under quasi-container-less conditions (Manara et al., 2008), a technique already employed for the study of several refractory materials (e.g.: Manara et al., 2005; Ronchi and Hiernaut, 1996; Manara et al., 2008; De Bruycker et al., 2010; Böhler et al., 2012; Manara et al., 2012), although in their micro-or macro-structured forms only. In the current research, this experimental method has been coupled to fast pyrometry and a laser-probe technique aimed at detecting the appearance of a liquid phase on the solid surface.

2. Materials and methods

2.1. Preparation of UO_2 nano-materials

UO_2 nanoparticles used in the present study have been produced through an aqueous process based on the electrochemical reduction of U(VI) into U(IV) and the precipitation of UO_2 in reducing and anoxic conditions at a constant pH (Jovani-Abril et al., 2011).

Due to the high surface-to-volume ratio the small nanoparticles produced oxidised immediately, so they were heat-treated at 900 K under reducing atmosphere (Ar + 6% H_2). This caused heterogeneous grain growth starting from 5 nm to (30 ± 20) nm, as calculated from the analysis of Transmission Electron Microscopy (TEM) images reported in Fig. 1. The powder was then cold-pressed obtaining pellets with weight between 300 mg and 425 mg.

2.2. Melting of nano-crystalline UO_2

None of the techniques so far used to study the melting point depression of nanoparticles (nano-calorimeters, high-temperature X-ray diffraction or *in situ* Electron Microscopy etc.) is applicable for high-melting materials such as actinide oxides. Bulk- refractory oxides have been successfully melted using sub-second laser heating coupled with pyrometry (e.g.: Manara et al., 2005, 2008, 2012; Ronchi and Hiernaut, 1996; De Bruycker et al., 2010; Böhler et al., 2012). Here the technique is applied for the first time to melt nano-structured actinide oxides.

The tuneable (up to the millisecond regime) fast heating of this experimental approach is crucial in order to limit pre-melting grain agglomeration and growth and study the melting point depression as a function of the grain size. The sample, held in an autoclave under controlled atmosphere, is heated by a 4.5 kW cw Nd:YAG TRUMPF® laser. Its power vs. time profile is programmable with a resolution of 1 ms. The onset of melting is detected by the appearance of vibrations in the signal of a probe laser (Ar^+ laser) reflected by the sample surface (Reflected Light Signal technique, or RLS) (Manara et al., 2008). The sample cools naturally when the laser beam is switched off. Thermal arrests corresponding to solidification can then be observed on the thermograms recorded by fast pyrometers. These operate in the visible-near infrared range between 488 nm and 900 nm. The reference pyrometer wavelength is here 655 nm. This was calibrated according to the procedure reported in (Manara et al., 2008; Böhler et al., 2012).

The normal spectral emissivity of urania has been assumed to be equal to 0.83, as determined from previous work (Manara et al., 2005). This value has been cross-checked in the current work with the help of a multi-wavelength spectro-pyrometer. Uncertainty of the measurements was calculated according to the error propagation law (Manara et al., 2008), taking into account the uncertainty associated to pyrometer calibration, to the emissivity, the transmittance of the optical system and the accuracy in detecting the onset of vibrations in the RLS signal. The estimated cumulative uncertainty is thus ±1% of the reported temperatures in the worst cases, with a $1 - k$ coverage factor. In Fig. 2 is given a schematic of the current laser heating experimental set-up.

2.3. Material characterisation

Detailed characterization of the material grain structure and its evolution after laser heating/melting has been an essential part of this work. Techniques employed to this goal are: PXRD, Thermo-Gravimetric Analysis (TGA), Scanning Electron Microscopy (SEM) and Transmission Electron Microscopy (TEM). PXRD were performed with a Bruker® D8 Advance diffractometer (Cu-Ka1

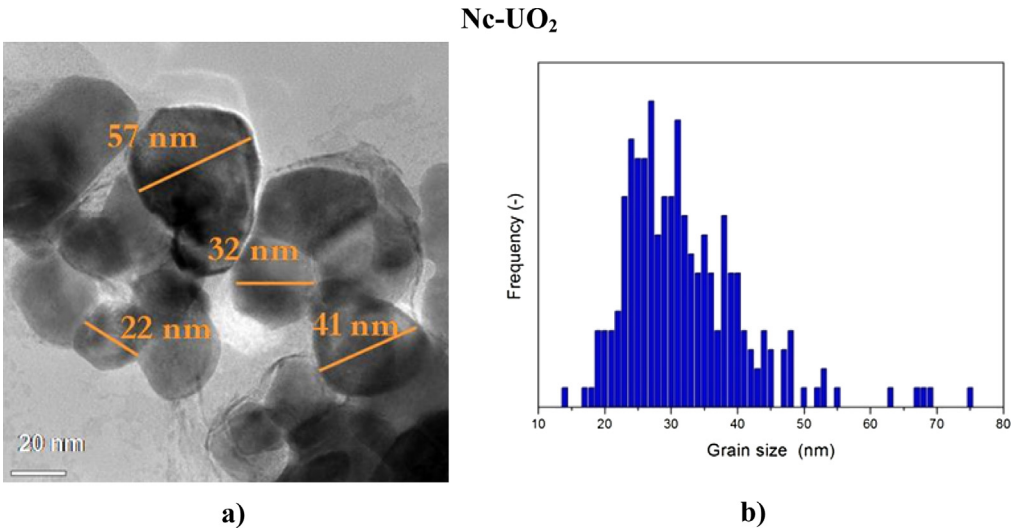

Fig. 1. TEM image of nano-crystalline UO_2 grains (a) and their size distribution analysis, yielding (30 ± 20) nm (b).

radiation) with a 2θ range of 10°–120° using 0.009° steps with 2 s of integration time per step at operating conditions of 40 kV to 40 mA.

SEM and EDS analyses were performed using a Phillips® XL 40 SEM operated at 25 kV and equipped with a SAMx EDS SD-Detector. High Resolution TEM investigations were done using a FEI® Tecnai G^2 F20 XT S/TEM operating at 200 kV, with a resolving power up to 1.8 Å, equipped with a EDAX EDS-System, and a Gatan® Tridiem imaging filter.

3. Results

Nc-UO_2 samples were laser heated beyond melting in a Ar + 6% H_2 gas pressurised to 0.3 MPa, in order to minimise massive vaporisation and avoid uncontrolled oxidation of the surface. Fig. 3 reports a thermogram recorded on a laser heated nc-UO_2 sample, compared with a thermogram obtained on a bulk standard UO_2 sample laser melted under the exact same conditions. The reflected light signal curve relative to nc-UO_2 is also shown in the same graph, where the appearance and disappearance of vibrations reveal the onset of melting on the sample surface. Instabilities are visible in both measured thermograms at high temperature, due to fast vaporisation and, possibly, local sample breaking. Independently it can be observed, with the help of the RLS, that liquid formation occurs in nc-UO_2 at (2750 ± 40) K, a much lower temperature than the bulk-UO_2 melting point. On the cooling stage solidification arrests are visible in both thermograms. However, a double inflection is visible in the nc-UO_2 curve, whereas the bulk UO_2 thermogram displays a simple thermal arrest preceded by some liquid undercooling. The double inflection of nc-UO_2 corresponds to a non-congruent melting/freezing transition, typical of hyper-stoichiometric uranium dioxide (Manara et al., 2005), and indicates that the O/U molar ratio ≠ 2 in such sample. It is a hard task to establish the exact O/U molar ratio at high temperature, knowing that it can considerably deviate from the original composition due to large non-congruent vaporisation (Guéneau et al., 2012, 2011). For this purpose, the nc-UO_2 thermogram has been compared with thermograms recorded under identical experimental conditions on three bulk UO_{2+x} samples with O/U molar ratio = 2.09, 2.13 and 2.20 (Fig. 3b shows only the thermograms of $UO_{2.09}$ and $UO_{2.13}$). These samples were produced by oxidising commercial UO_2 pellets under a controlled oxygen

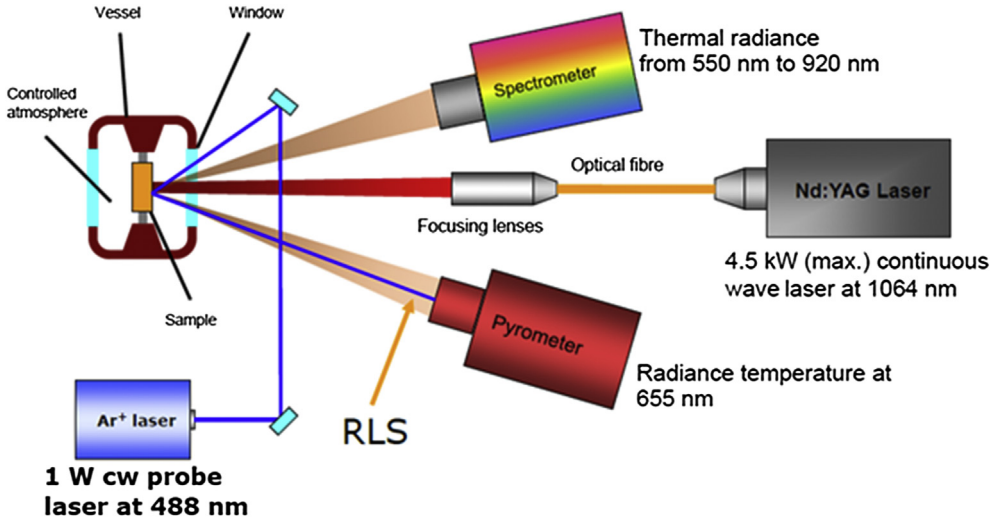

Fig. 2. Laser heating technique, experimental set-up.

potential (Manara et al., 2005). Fig. 3 shows that the solidification thermogram of nc-UO_2 lies somewhat in between those of the samples with starting compositions $UO_{2.09}$ and $UO_{2.13}$, as expected from the pre-melting characterisation. Of course the oxidation state of these latter specimens changed as they were laser melted under a reducing atmosphere. For this reason the melting onset temperatures observed by RLS are slightly shifted in the three cases, although still comparable. By comparison with the solidus/liquidus lines measured in (Manara et al., 2005) under a high buffer gas pressure (He at 1 MPa), the O/U molar ratio after the melting/freezing cycle in the bulk samples $UO_{2.09}$ and $UO_{2.13}$ have been estimated to be 2.07 and 2.08 respectively. For this specific nc-UO_2 sample, the composition at which the melting/solidification transition occurred can be situated between these two O/U molar ratio values. However, by repeating the same procedure on other similar nc-UO_2 samples, such result was reproduced only within a larger uncertainty.

Table 1 reports a summary of the temperatures at which onset of liquid state was detected in nano-structured uranium dioxide pellets. Furthermore, liquidus and solidus temperature corresponding to thermogram inflections on the cooling stage are given. All shots were performed in Ar/H_2. In case a second shot on the "fresh" rear side of the sample was performed the melting temperature systematically increased: it is likely that both a reduction of the sample and a partial agglomeration of the nano-grains took place during the first heating/cooling cycle.

Comparing solidus and liquidus temperatures with the values of bulk UO_{2+x}, the final oxidation state can be assessed to be in the range $0.05 < O/M < 0.12$ for nc-uranium dioxide. Such a large uncertainty can be attributed to an inhomogeneous oxidation state in different samples. This is a logical consequence of the high reactivity of this nano-crystalline material, linked to its large specific surface. The measured melting points have an average of 2790 K and a standard deviation of 60 K.

Table 1
Summary of laser heating results obtained for nc-UO_2.

Sample	$T_{melting}$/K	δT/K	$T_{liquidus}$/K	δT/K	$T_{solidus}$/K	δT/K
NCP1	2750	37	3160[b]	50	3024	42
	2813[a]	38	3124	44	–	
NCP2	2736	37	2924	40	2794	38
	2845[a]	39	Broken	–	–	
NCP5[c]	Not detected	–	3080	43	3000	42
NCP6[c]	2820	38	3098	43	3039	42

[a] Second shot on the sample's rear surface.
[b] The inflection temperature (3160 K) is doubtful due to vaporisation and sample breaking.
[c] An in situ laser heat treatment up to around 1300 K was performed (45 W × 10 s) in order to try to remove the surface likely to be over-oxidised. It is possible that some crystallite growth occurred before the laser melting shot.

4. Discussion

It is obvious from the results reported in Fig. 3, that the melting behaviour of the investigated nc-compound is significantly different from the one observed in bulk material of the same nature. However, composition changes were likely to happen during the laser heating experiments, due to the poor chemical stability of urania, even worsened by the large specific surface of the current nc-samples. PXRD analysis was performed on them both before and after melting experiments. The O/U molar ratio after the reducing annealing treatment (before laser heating) was estimated to be 2.10 ± 0.02 from the XRD peak maximum position and TGA analyses. The XRD peak maxima were considered to be corresponding to a single UO_{2+x} phase and the formula reported in Grønvold (1955) was used to obtain O/U molar ratio $= 2 + x$ from the evolution of the lattice parameter a:

$$a(\text{nm}) = 0.54705 - 0.0094x \quad (3)$$

PXRD actually shows broad peaks shifted towards higher angles compared to the pattern measured from commercial bulk UO_2 (Fig. 4(a)). The XRD pattern is also compared to that of bulk UO_{2+x}, and looks very different from those, too. Since a size effect causes a clear contraction of the lattice parameter, already measured for nc-UO_2 (Jovani-Abril et al., 2011), the resulting peak broadening hindered any more precise quantification of the O/U molar ratio here because the characteristic peaks of the different phases are undistinguishable.

After laser heating peaks are less broad because of the grain growth (Fig. 4(b)). A shoulder due to the presence of the additional pattern of the homomorphous fcc U_4O_9 phase is visible, though the two peaks are still not clearly resolved. This result confirms that a considerable grain growth (from nanoscopic to microscopic) has occurred in the laser heated specimens. Together with the RLS and SEM evidence, and, even more, the fact that a clear freezing thermal arrest was observed on the cooling flank of the thermograms, this constitutes a sound proof that melting really occurred on those samples. As mentioned in the result section, comparing the nc-UO_2 solidification arrests with those of standard UO_{2+x} samples was probably the best way to estimate the actual composition at which

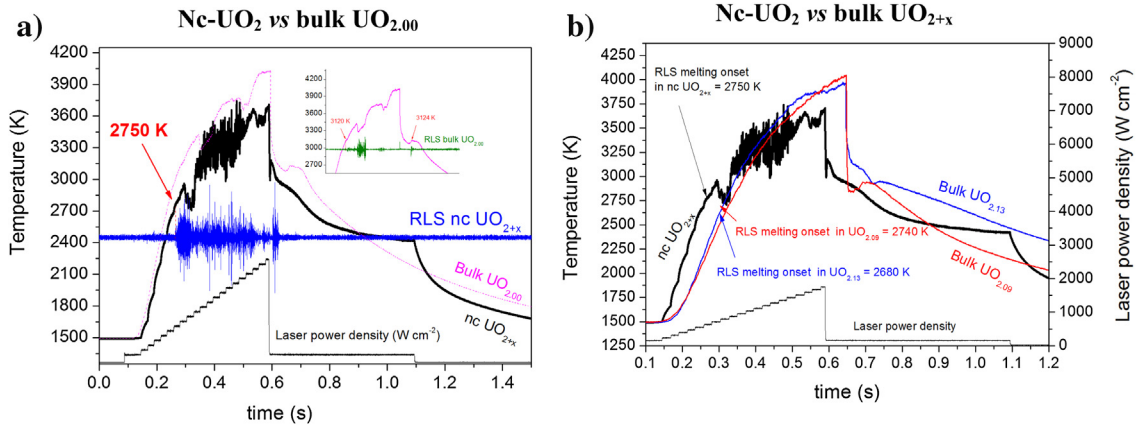

Fig. 3. Laser heating of UO_2. a) Comparison between thermograms and Reflected Light Signals (RLS) recorded on an nc UO_2 sample and a bulk $UO_{2.00}$ sample, both heated beyond melting; b) Comparison between a thermogram recorded on a nc sample and those measured on bulk $UO_{2.08}$ and $UO_{2.13}$ samples, all heated beyond melting. Melting onset temperatures are indicated in the three cases, but RLS is not shown here for the sake of a better readability.

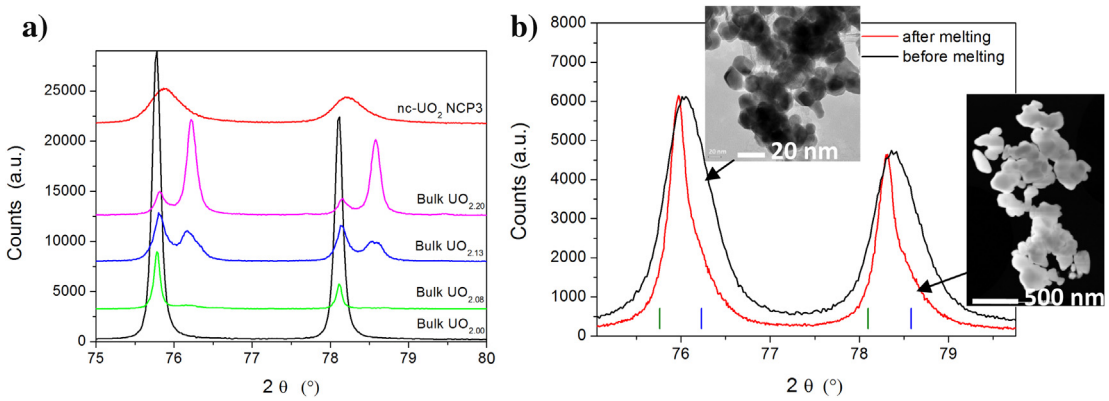

Fig. 4. Magnification of PXRD patterns of (a) Ar/H_2 annealed nc-UO_2 before laser heating compared with bulk UO_2 and bulk UO_{2+x} samples; (b) Ar/H_2 annealed nc-UO_2 before laser heating and the same sample after laser melting. The positions of U_4O_9 characteristic peaks (blue lines) and UO_2 characteristic peaks (green lines) are indicated by vertical lines at the graph bottom. (For interpretation of the references to color in this figure legend, the reader is referred to the web version of this article.)

the melting/freezing transition occurred. In fair agreement with the other pre- and post-melting analyses, this composition has been estimated to be $UO_{2.08\pm0.03}$, slightly reduced with respect to the initial composition due to the Ar/H_2 atmosphere under which the laser heating tests were performed. According to literature data, for bulk urania melting of compositions in the range $UO_{2.08\pm0.03}$ should occur between 2700 K and 2900 K (Manara et al., 2005; Guéneau et al., 2011). Obviously, the melting point of nc-UO_2 observed in the current work falls in the same temperature range. Therefore, it should be concluded that whereas a slight size effect is likely to exist in the current (30 ± 20)-nm grained uranium dioxide samples, it cannot be distinguished from the melting temperature depression due to oxygen hyper-stoichiometry. This conclusion is in qualitative agreement with the literature data (Buffat and Borel, 1976; Lai et al., 1998), that a significant melting point depression was visible in Au and Al nanoparticles only in crystallites smaller than approximately 10 nm to 20 nm.

It would in principle be possible to obtain similar conclusions about the size dependence of the melting point of the materials investigated in this research theoretically, with the help of Eq. (2) above. However, the estimation of the parameter α for melting urania is extremely difficult because the necessary high-temperature thermophysical data are scanty and uncertain (cf. Fink, 2000).

The high temperature properties, and in particular the melting behaviour, of the current kind of material are definitely different from those of the same compound in its bulk-form. It is however clear, that already crystallites with an average size of 30 nm have only an indirect effect on the melting point depression (one would therefore expected an even smaller effect in crystallites larger than 100 nm, as those studied by Spino et al. (2012). Still, their nanoscopic dimensions imply a large specific surface, and therefore a poorer resistance towards oxidation. It is the consequent hyper-stoichiometry, systematically produced in nc-UO_2, that leads to a lower melting point.

In order to clarify the sole effect of grain dimension on the melting temperature depression in refractory oxides, the chemically more stable ThO_2 is currently under study in its nanocrystalline form. Nano-crystalline ThO_2 pellets have been obtained using nanoparticles with very small grain size produced through non-aqueous synthesis (Hudry et al., 2012, 2013).

5. Conclusions

Nano-crystalline (nc) uranium dioxide has been laser heated and successfully melted in the present research.

Nc-UO_2 samples with an average crystallite size of 30 nm have been investigated with the aim of giving conservative data possibly comparable with the smallest grain size detected in the high burn-up structure.

The following conclusion can be drawn: nano-structured (30 nm ± 20 nm) uranium dioxide melts at 2790 K ± 60 K instead of 3120 K ± 30 K established for bulk-UO_2. This is mostly attributable to fast oxidation, leading to a melting/freezing composition (even in Ar + 6% H_2 at 0.35 MPa) of $UO_{2.08\pm0.03}$. For nano-crystals of the order of a few tens nm, the grain-size melting depression effect is of the same order as the experimental uncertainty relative to the determination of the solid/liquid transition. The most remarkable high-temperature effects of the nanoscopic grain structure here studied, compared to the bulk form, are the poorer stability towards fast vaporisation and oxidation. The issue of the enhanced oxidation of nano-structured UO_2 will be treated in detail in future research. From the current results, it seems already reasonable to conclude that no significant depression of the melting point of nc-UO_2 with mean grain size reproducing the high burn-up structure (150 nm–300 nm) is to be expected.

The current results open the way to further investigation, the ultimate goal of which should be the assessment of a grain-size dependence of the melting temperature of nano-structured UO_2.

Experimental characterisation of nano-crystalline ThO_2 at high temperature, beyond melting, is on-going. ThO_2 is in fact chemically more stable than UO_2 and therefore probably more suited for the detection of a pure grain-size effect.

Acknowledgements

The authors are indebted to P. Lajarge, A. Guiot and S. Gardeur (JRC-ITU) for performing heat treatments on the nc-UO_2 samples, G. Pagliosa, D. Bouexière, M. Ernstberger, B. Cremer (JRC-ITU) and E. Courtois (KIT–INT) for the sample characterisation, R. Böhler and P. Cakir (JRC-ITU) for their help in the laser heating experiments. Special thanks are conveyed to V.V. Rondinella, R.J.M. Konings, J. Somers, P. Raison, T. Wiss (JRC-ITU) and C.E. Bottani (Politecnico di Milano) for their scientific advice.

References

Böhler, R., Welland, M.J., De Bruycker, F., Boboridis, K., Janssen, A., Eloirdi, R., Konings, R.J.M., Manara, D., 2012. Revisiting the melting temperature of NpO_2 and the challenges associated with high temperature actinide compound measurements. J. Appl. Phys. 111, 113501–113508.

Buffat, P., Borel, J.-P., 1976. Size effect on the melting temperature of gold nanoparticles. Phys. Rev. A 13, 2287–2296.
Coombes, C.J., 1972. The melting of small particles of lead and indium. J. Phys. F 2, 441–449.
De Bruycker, F., Boboridis, K., Manara, D., Poeml, P., Rini, M., Konings, R.J.M., 2010. Reassessing the melting temperature of PUO_2. Mater. Today 13, 52–55.
Fink, J.K., 2000. Thermophysical properties of uranium dioxide. J. Nucl. Mater. 279, 1–18.
Grønvold, F., 1955. High temperature X-ray study of uranium oxides in the UO2-U3O8 region. J. Inorg. Nucl. Chem. 1, 357–370.
Guéneau, C., Dupin, N., Sundman, B., Martial, C., Dumas, J.-C., Gossé, S., Chatain, S., De Bruycker, F., Manara, D., Konings, R.J.M., 2011. Thermodynamic modelling of advanced oxide and carbide nuclear fuels: description of the U–Pu–O–C systems. J. Nucl. Mater. 419, 145–167.
Guéneau, C., Chartier, A., Brutzel, L.V., 2012. Thermodynamic and thermophysical properties of the actinide oxides. In: Konings, R.J.M. (Ed.), Compre. Nucl. Mater, first ed. Elsevier, Amsterdam.
Guisbiers, G., 2012. Review on the analytical models describing melting at the nanoscale. J. Nanosci. Lett. 2, 8.
Hill, T.L., 2001. A different approach to nanothermodynamics. Nano Lett. 1, 273–275.
Hudry, D., Apostolidis, C., Walter, O., Gouder, T., Courtois, E., Kübel, C., Meyer, D., 2012. Non-aqueous synthesis of isotropic and anisotropic actinide oxide nanocrystals. Chem. Eur. J. 18, 8283–8287.
Hudry, D., Apostolidis, C., Walter, O., Gouder, T., Courtois, E., Kübel, C., Meyer, D., 2013. Controlled synthesis of thorium and uranium oxide nanocrystals. Chem. Eur. J. 19, 5297–5305.
Jovani-Abril, R., Eloirdi, R., Bouexière, D., Malmbeck, R., Spino, J., 2011. In situ high temperature X-ray diffraction study of UO_2 nanoparticles. J. Mater. Sci. 46, 5–10.
Lai, S.L., Guo, J.Y., Petrova, V., Ramanath, G., Allen, L.H., 1996. Size-dependent melting properties of small tin particles: nanocalorimetric measurements. Phys. Rev. Lett. 77, 99–102.
Lai, S.L., Carlsson, J.R.A., Allen, L.H., 1998. Melting point depression of Al clusters generated during the early stages of film growth: nanocalorimetric measurements. Appl. Phys. Lett. 72, 1098–1100.
Manara, D., Ronchi, C., Sheindlin, M., Lewis, M., Brykin, M., 2005. Melting of stoichiometric and hyperstoichiometric uranium dioxide. J. Nucl. Mater. 342, 148–163.
Manara, D., Sheindlin, M., Heinz, W., Ronchi, C., 2008. New techniques for high-temperature melting measurements in volatile refractory materials via laser surface heating. Rev. Sci. Instrum. 79, 1139011–1139017.
Manara, D., Böhler, R., Boboridis, K., Capriotti, L., Quaini, A., Luzzi, L., De Bruycker, Guéneau, C., Dupin, N., Konings, R., 2012. The melting behaviour of oxide nuclear fuels: effects of the oxygen potential studied by laser heating. Proc. Chem. 7, 505–512.
Mei, Q.S., Lu, K., 2007. Melting and superheating of crystalline solids: from bulk to nanocrystals. Progr. Mater. Sci. 52, 1175–1262.
Nogita, K., Une, K., 1994. Nucl. radiation-induced microstructural change in high burnup UO2 fuel pellets. Instr. Meth. Phys. Res. B 91, 301–306.
Olander, D.R., 1976. Fundamental Aspects of Nuclear Reactor Fuel Elements. Technical Information Center, Office of Public Affairs Energy Research and Development Administration, New York.
Roduner, E., 2006. Nanoscopic Materials: Size-dependent Phenomena. RSC Publishing.
Ronchi, C., Hiernaut, J.P., 1996. Experimental measurement of pre-melting and melting of thorium dioxide. J. Alloy Comp. 240, 179–185.
Ronchi, C., Sheindlin, M., Staicu, D., Kinoshita, M., 2004. Effect of burn-up on the thermal conductivity of uranium dioxide up to 100.000 MWd t^{-1}. J. Nucl. Mater. 327, 58–76.
Rondinella, V.V., Wiss, T., 2010. The high burn-up structure in nuclear fuel. Mater. Today 13, 24–32.
Spino, J., Vennix, K., Coquerelle, M., 1996. Detailed characterisation of the rim microstructure in PWR fuels in the burn-up range 40–67 GWd/tM. J. Nucl. Mater. 231, 179–190.
Spino, J., Cobos-Sabate, J., Rousseau, F., 2003. Room-temperature microindentation behaviour of LWR-fuels, part 1: fuel microhardness. J. Nucl. Mater. 322, 204–216.
Spino, J., Santa Cruz, H., Jovani-Abril, R., Birtcher, R., Ferrero, C., 2012. Bulk-nanocrystalline oxide nuclear fuels – an innovative material option for increasing fission gas retention, plasticity and radiation tolerance. J. Nucl. Mater. 422, 27–44.
Takagi, M.J., 1954. Electron diffraction study of liquid–solid transition of thin metal films. J. Phys. Soc. Jpn. 9, 359–363.
Wronski, C.R.M., 1967. The size dependence of the melting point of small particles of tin. Br. J. Appl. Phys. 18, 1731–1737.